Research Article

Moorthy Muruganandham, Kanagasabapathy Sivasubramanian*, Palanivel Velmurugan, Natarajan Arumugam, Abdulrahman I. Almansour, Raju Suresh Kumar, Sakkarapalayam M. Mahalingam, and Subpiramaniyam Sivakumar*

Phytocrystallization of silver nanoparticles using *Cassia alata* flower extract for effective control of fungal skin pathogens

https://doi.org/10.1515/gps-2023-0013
received January 27, 2023; accepted May 07, 2023

Abstract: A feasible alternative to classic chemical synthesis, the phyto-mediated production of silver nanoparticles (AgNPs) utilizing aqueous flower petal extract of *Cassia alata* as a reducing agent is reported for the first time. Characterization of synthesized AgNPs was carried out using various techniques *viz*., ultraviolet-visible spectroscopy (UV-Vis), X-ray powder diffraction (XRD), high-resolution transmission electron microscope (HRTEM), Fourier transform infrared spectroscopy (FTIR), and scanning electron microscopy (SEM) with energy dispersive X-ray analysis (EDX). The results of the FTIR research conducted in this study show different bond stretches with varying durations, which can be seen at various faraway points. AgNPs are mainly spherical and vary in size from 20 to 100 nm, according to TEM images. The highest X-ray energy surge, at 3 keV, is visible in the EDX spectrum. The XRD pattern showed that four diffraction peaks could be assigned to the 111, 200, 220, and 311 planes of the face-centered cubic crystalline silver, respectively, at 32.05, 46.27, 55.25, and 57.39°. Optimization of production parameters including pH, metal ion concentration, and substrate concentrations were studied. In addition, the bioactivity was evaluated against *Trichophyton rubrum*, *Aspergillus fumigatus*, *Candida albicans*, *Epidermophyton floccosum*, and *Mucor* sp. using the agar diffusion method. Furthermore, their antioxidant properties were assessed using 2,2-diphenyl-1-picryl-hydrazyl-hydrate assay and ferric ion reducing antioxidant power tests. MTT assay was performed using human fibroblast cell line (L929) to determine the cell viability and cytotoxicity through increased metabolism of the tetrazolium salt.

Keywords: *Cassia alata* flower, phyto compound, silver, biomedical, applications

*** Corresponding author: Kanagasabapathy Sivasubramanian,** Department of Microbiology, Sri Sankara Arts and Science College, Kanchipuram, Tamil Nadu, India; Centre for Materials Engineering and Regenerative Medicine, Bharath Institute of Higher Education and Research, Selaiyur, Chennai, Tamil Nadu 600126, India, e-mail: skssmani2018@gmail.com
*** Corresponding author: Subpiramaniyam Sivakumar,** Department of Bioenvironmental Energy, College of Natural Resources and Life Science, Pusan National University, Miryang-si, Gyeongsangnam-do 50463, Republic of Korea, e-mail: ssivaphd@yahoo.com
Moorthy Muruganandham: Department of Microbiology, Sri Sankara Arts and Science College, Kanchipuram, Tamil Nadu, India; Centre for Materials Engineering and Regenerative Medicine, Bharath Institute of Higher Education and Research, Selaiyur, Chennai, Tamil Nadu 600126, India
Palanivel Velmurugan: Centre for Materials Engineering and Regenerative Medicine, Bharath Institute of Higher Education and Research, Selaiyur, Chennai, Tamil Nadu 600126, India
Natarajan Arumugam, Abdulrahman I. Almansour, Raju Suresh Kumar: Department of Chemistry, College of Science, King Saud University, P.O. Box 2455, Riyadh 11451, Saudi Arabia
Sakkarapalayam M. Mahalingam: Department of Chemistry, Purdue University, 720 Clinic Drive, West Lafayette, Indiana 47907, USA

1 Introduction

Multidrug resistance (MDR) has become an increasingly severe threat to humans on a worldwide scale. According to MDR, an organism is not susceptible to at least one substance from three or more antimicrobial groups [1]. Due to their distinct biological, molecular, and physical characteristics, silver nanoparticles (AgNPs) have become more popular among different biosynthesized metal nanoparticles (NPs) over the past 20 years [2]. Despite the fact that silver is toxic at higher concentrations, numerous studies have shown that $AgNO_3$ has greater chemical stability, catalytic activity, biocompatibility, and inherent curative potential at lower concentrations [3]. It has been suggested that silver nanoparticles may have antibacterial and carcinogenic properties [4]. In fact, one of the silver

nanoparticles' most notable benefits over mass metals and their salts is the controlled and gradual discharge of silver from the particles [5]. The new-age bio-nanoformulations' guiding principle is the integration of conventional medicine and nanotechnology. Physical techniques – the two most significant physical methods are laser ablation and evaporation-condensation. Atmospheric pressure physical synthesis of AgNPs has some drawbacks. For instance, the tube furnace takes up a lot of room, uses a lot of energy while raising the temperature around the source material, and takes a long time to reach thermal stability. Additionally, a normal tube furnace needs to be preheated for several minutes and uses more than a few kilowatts of electricity to achieve a stable working temperature [6,7]. Chemical reduction, the most popular technique for creating NPs, uses an organic solvent like ethylene glycol [8], ascorbate [9], sodium borohydride [10], and hydrazine [11]. Since chemical reduction produces poor yields, it necessitates complicated purification processes and consumes a lot of energy; hence, there was a genuine need for the creation of cleaner and safer methods. This led to the development of green synthesis, in which plant extracts are used to reduce silver to silver nanoparticles.

Numerous plant and medicinal products have reportedly been used in the green method of synthesizing NPs, which has been reported to have low or no toxicity [12]. Plant samples contain a variety of secondary metabolites that serve as reducing or capping agents during the production of NPs [13]. Several studies have been reported on the pharmaceutical and biological potential of green synthesized silver nanoparticles such as antibacterial and biofilm inhibitory activities [14], antifungal [15], antiparasitic, antioxidant, anticoagulant [16], and antiviral [17]. Further, anticancer activity of biosynthesized AgNPs was assessed against various cancers such as lung [18], colorectal [19], leukemia [20], hepatic [21], etc. *Cassia alata*, also known as candle bush, wild senna, ringworm senna, among others, is an annual tropical plant with leathery, complex leaves that belongs to the Caesalpiniaceae family. The leaves are laxative and have potent antibacterial and antifungal qualities [22]. The leaves treat dermatophyte infections like "tide afoot," also known as "athlete foot," superficial mycoses, and chronic fungal illnesses like "pityriasis versicolor." *C. alata* is an effective treatment for ringworm as well as a number of other skin conditions, including eczema and chronic skin problems [23]. The main fungi that cause skin infections are dermatophytes, particularly the *Trichophyton* and *Microsporum* types. There are numerous fungi that can induce surface mycoses, including *T. rubrum*, *T. mentagrophytes* var. *interdigitale*, and *M. canis*. Other species, like *T. soudanense* (Africa), *T. schoenleinii* (Eurasia and Africa), *T. violaceum* (Asia, Africa, and Europe), and *T. concentricum*, are limited by geographic area (Pacific Islands, India, and far East) [24]. In the current study, silver nitrate ($AgNO_3$) was reduced to AgNPs using *Cassia alata* flower extract. The synthesized NPs were then characterized using a variety of techniques, including X-ray diffraction (XRD), transmission electron microscopy (TEM), energy-dispersive X-ray spectroscopy (EDX), and Fourier transform infrared spectroscopy (FT-IR) and their bioactivity effect on fungal skin pathogens were estimated. Additionally, antioxidant and anticancer potential were analyzed using human fibroblast cell line L929 through MTT assay. The novelty of this study lies in the fact that minimal NP sizes and the simplified synthetic method of AgNPs were attained using a rich phytochemical from the flower of a traditional medicinal plant *C. alata*. Additionally, an eco-friendly method using aqueous extracts for the production of AgNPs has been developed.

2 Materials and methods

2.1 Collection and preparation of samples

The *C. alata* plant flower was freshly collected from Enathur village (latitude 12.84°N and longitude 79.73°E) in Kanchipuram, Tamil Nadu, India. The *C. alata* flower petals were cut into small pieces using sterile scissors and the surface of the flower was washed with sterile distilled water. About 50 g flower was soaked in 100 mL of distilled water and boiled in a heating mantle for 30 min at 100°C using a 500 mL beaker. Then, the extract was cooled, filtered with a muslin cloth and then with Whatman No. 1 filter paper. The extract was stored at 4°C for further use.

2.2 Phytochemical analysis of *C. alata* flower extract

One milliliter of extract, 2 mL of distilled water, and a few drops of 10% aqueous $Fecl_3$ were added to the mixture. The appearance of a brown color denotes the presence of flavonoids, whereas the appearance of a blue or green color denotes the presence of phenols. After mixing together 5 mL of extract, 2 mL of chloroform, and 3 mL of strong sulfuric acid, a color that was described as reddish-brown at the interface indicated the presence of terpenoids. After dissolving 1 mL of the extract in 1 mL of glacial acetic acid, the mixture was allowed to cool, and

then 2–3 drops of ferric chloride were added. 2 mL of concentrated H_2SO_4 was added. At the point where two layers meet, the presence of glycosides can be identified by the formation of a ring that is reddish-brown in color. Following the addition of 2 mL of hydrochloric acid to 1 mL of extract, the resulting liquid was heated in a water bath for 15 min, after which it was allowed to cool before being filtered. After treating the filtrate with a 10% solution of potassium hydroxide, the aqueous layer turned a pinkish-red color, which is evidence that anthraquinones are present. The filtrate was combined with chloroform. After adding 1 mL of strong sulfuric acid to 1 mL of extract, a red tint was produced, which is a telltale sign that quinones are present. Every active phytochemical analysis was carried out using the method followed by Jayasree et al. [25].

2.3 Biosynthesis of AgNPs

For the biogenesis of AgNPs, a solution of $AgNO_3$ with a concentration of 0.1 mM was utilized. After thoroughly combining the ingredients at room temperature, 1 mL of aqueous floral extract was added to 9 mL of a solution containing 0.1 mM of $AgNO_3$. There was a noticeable shift in the brown color. Measurements in UV-visible (UV-Vis) spectroscopy were taken on a regular basis in order to keep an eye on how the silver ions in the solution were being bio-reduced (300–800 nm). The creation of a solution with a color that was somewhere between reddish-brown and brown color showed the morphology of the AgNPs [26].

2.4 Optimization of green synthesis of AgNPs

2.4.1 Different pH

1.0 mL of *C. alata* flower aqueous extract and 9.0 mL of 0.1 mM $AgNO_3$ were added and maintained at different pH (3, 4, 5, 6, 7, 8, 9, and 10) at room temperature and observed for brown color changes. The absorbance of the resulting solutions was measured between 300 and 800 nm using a UV-Vis spectrophotometer [27].

2.4.2 Different concentrations of $AgNO_3$

To 1.0 mL of *C. alata* flower aqueous extract, 9.0 mL of $AgNO_3$ (pH 9.0) was added at different concentrations such as 100, 200, 300, 400, and 500 mM and incubated at ambient temperature. The absorbance of the resulting solutions was measured by the UV-Vis spectrophotometer [27].

2.4.3 Different concentrations of substrate (flower extract)

Different volumes of *C. alata* flower aqueous extract such as 0.5, 1, 1.5, 2, and 2.5 mL were taken and made up to 10 mL containing 0.1 mM $AgNO_3$ (pH 9.0) for the synthesis of AgNPs at ambient temperature. The absorbance of the resulting solutions was measured by the UV-Vis spectrophotometer [27].

2.5 Synthesis of AgNPs

Synthesis of AgNPs was achieved by using conditions with pH, substrate, and $AgNO_3$ concentrations that were all optimized. Following the completion of the mass production, the solution containing the AgNPS was subjected to multiple rounds of centrifugation at a speed of 12,000 rpm for a period of 30 min. The characterization study was performed on the pellet after it had been dried in an oven with hot air.

2.6 Characterization of synthesized AgNPs

The synthesized bio-reduced AgNPs were characterized by utilizing a UV-Vis spectrophotometer, and the results were based on an analysis of the concentrations of pH, substrate, and $AgNO_3$. After placing the sample in a quartz cuvette, measurements of optical density (OD) at wavelengths ranging from 300 to 800 nm were performed, and the findings were recorded [25]. Using Fourier Transform Infrared (FTIR) spectroscopy, the biomolecules that were found to be present in the AgNPs that were made using the flower extract of *C. alata* were determined. The FTIR was captured over a spectrum that extended from 500 to 4,000 cm^{-1}. The different modes of vibration that were found in the AgNPs were catalogued and categorized so that a specific functional group could be determined [26].

We used a JEOL JEM-2011 transmission electron microscopy (TEM) with an accelerating voltage of 200 kV to determine the size, shape, and particle size distributions of the particles. In order to prepare samples for TEM

examination, a drop of the solution was placed on a carbon-coated copper grid, and then the grid was allowed to dry in the air. For the examination of energy dispersal, EDX spectrum was analyzed to determine the elemental composition of the synthesized AgNPs [28]. Analysis of X-ray diffraction patterns (XRD) also revealed the crystalline character of the green AgNPs that were generated by the *C. alata* flower extract. An XRD examination was performed, which resulted in the determination of the AgNPs' crystalline nature, as well as their size and phase identification. The instrument was set to operate at a voltage of 40 kV and a current of 30 mA, and it used CuK1 radiation in –2 configurations. The crystallite domain size was determined by taking the width of the XRD peaks and applying the formula developed by Scherrer, which is $D = K\lambda/\beta\cos\theta$. In this equation, D represents the average crystallite domain size perpendicular to the reflecting planes, K is the Scherrer constant, λ is wave length of the X-ray beam used (1.54,184 Å), β is the Full width at half maximum (FWHM) of the peak and θ is the Bragg angle [29].

2.7 Biomedical applications

2.7.1 Antifungal activity

To cultivate the pathogenic fungus, including *Trichophyton rubrum*, *Aspergillus fumigatus*, *Candida albicans*, *Epidermophyton floccosum*, and *Mucor* sp., the Sabuoraud dextrose agar (SDA) plates were prepared according to the manufacturer's specification and then cooled. Using a sterile well puncher with a 5 mm diameter hole borer, holes were drilled into the culture media plate. Two of the wells had crude extract (25 and 50 µL) added to them, and the other two wells had AgNPs (25 and 50 µL) added. The positive controls, each consisting of 5 µL of nystatin, were carried out in triplicate. After allowing the plates to diffuse for 1 h, they were incubated for either 24 h (for *C. albicans*) or 120 h (*T. rubrum*, *A. fumigatus*, *E. floccosum*, and *Mucor* sp.). Finally, the plates were examined for zones of inhibition, and readings were taken in millimeters [30–32].

2.7.2 Determination of minimum fungicidal concentration (MFC)

To determine the MFCs, 1 mL of standardized inoculum spores of 1×10^7 CFU·mL^{-1} was mixed with Sabouraud dextrose broth and subsequently added the different concentrations of flower extract from 10–100 µg·mL^{-1}. Then, all the broths were incubated in aseptic conditions for 24–48 h. After 48 h, 0.1 mL of inoculums was withdrawn from each broth concentration and inoculated on SDA to examine MFC. Plates were incubated for 72 h. MFC was the lowest drug concentration that showed less than three colonies or no visible growth on the plates and is considered an inhibition activity of 99% or 100%, respectively [33,34].

2.8 Antioxidant activity

2.8.1 2,2-Diphenyl-1-picryl-hydrazyl-hydrate (DPPH) free radical scavenging assay

The free radical scavenging competence was performed using DPPH assay with some modification [35]. Just before the experiment, 0.1 M of DPPH and various concentrations of AgNPs (20–100 g·mL^{-1}), and aqueous flower extract (20–100 g·mL^{-1}) were prepared by dissolving in methanol. Each concentration of 1 mL was mixed separately with 1 mL of DPPH and the mixture was incubated for 30 min in a dark place. From each reaction mixture, 200 µL was transferred to a 96-well microtiter plate and by using the UV-Vis spectrophotometer, the absorbance was measured at 517 nm. AgNPs and flower petal aqueous extract were used in this triplicate test. The negative and positive controls were DPPH and ascorbic acid, respectively. Methanol was used as a blank for the experiment at the same time. The activity of radical scavenging was computed as follows:

$$\text{Free radical scavenging activity (\%)} = \frac{\text{Control Abs} - \text{Test sample (Abs)}}{\text{Control (Abs)}} \times 100 \quad (1)$$

2.8.2 Ferric ion reducing antioxidant power (FRAP) free radical scavenging assay

The FRAP activity of the synthesized AgNPs and aqueous extract at various concentrations was investigated using the method followed by Lal et al. [35] with minor changes. In short, 1 mL of various concentrations of AgNPs (20–100 g·mL^{-1}) and aqueous flower extract (20–100 g·mL^{-1}) were mixed individually in separate test tubes with 1 mL of 0.2 M sodium phosphate buffer, then 1 mL of 1% potassium ferricyanide was added and incubated for 20 min at 50°C water bath. Then, from the reaction mixture, 1 mL of each sample was pipetted out and mixed with 1 mL of dH_2O. After that, to each test tube,

0.2 mL of ferric chloride (0.1% in dH_2O) was added. 200 µL of final solution were collected from each concentration and placed into a 96-well microtiter plate. A multi-leader was used to measure the absorbance at 700 nm. The results were duplicated and recorded in triplicate for the aqueous flower extract. The blank was made the same way, but instead of dH_2O, 1% $K_3[Fe(CN)_6]$ was used. The positive control was ascorbic acid (20–100 $g{\cdot}mL^{-1}$). Each sample's antioxidant capacity was estimated using the linear ferrous sulphate calibration curve.

2.9 MTT assay using human fibroblast cell line L929

The MTT assay is a standard colorimetric non-radioactive assay that measures cytotoxicity and the number of live cells by observing the increase in the metabolism of the tetrazolium salt. Human fibroblast cell line (L929) was used to detect the cytotoxic effect of the biosynthesized AgNPs. After seeding fibroblast cells at a density of 1×10^5 $cells{\cdot}mL^{-1}$ onto 96-well plates, the plates were placed in an incubator for 24 h. Following this, the cells were exposed to various concentrations, ranging from 25 to 1,200 $\mu g{\cdot}mL^{-1}$. After that, the cells were kept at 37°C for 24 h while being exposed to 5% carbon dioxide. Following incubation, 0.5 $mg{\cdot}mL^{-1}$ of MTT was applied to the cells that had been incubated. After the end of incubation time, the cells were left to culture for a further 4 h. After that, 100 µL of DMSO was added to each well, and the contents were well combined and at the wavelength of 570 nm, absorbance was determined using a multimode reader.

2.10 Statistical analysis

All the assays were carried out in triplicate on each occasion. The data were presented as the mean value ± standard deviation (SD) from three separate trials.

3 Results and discussion

The use of nanotechnology in medicine seems to be a hopeful and successful strategy. Due to their distinct physicochemical characteristics, biogenic silver, and gold NPs in particular have garnered considerable interest for their anti-leukemic action. In fact, these nanostructures have shown promise in anti-leukemic uses, either as new therapeutic agents or as transporters to improve drug bioavailability and tailored distribution to a particular organ [20]. Flavonoids, phenols, cardiac glycosides, terpenoids, glycosides, and quinones (Table 1) were observed in the aqueous flower extraction of *C. alata*. It has been stated that *C. alata* is abundant in a wide variety of phytochemical elements, which are the active ingredients in the immune-enhancing activity. A comparable finding had been reported in the same plant, *C. alata*, which included anthraquinones that had been present in the current investigation [28].

3.1 Biosynthesis of AgNPs

As a result of the surface plasmon resonance phenomenon, the reduction of $AgNO_3$ into AgNPs that occurs during plant extraction process is followed by a progressive increase in color development starting from a clear reddish-brown (Figure 1d). The floral extracts that did not include any $AgNO_3$ did not exhibit any change in color.

3.2 Effect of different pH

At several pH levels, ranging from 3 to 10, brown color variations were observed (Figure 2a). Using a UV-Vis spectrophotometer, the absorbance of the resultant solutions was determined to be anywhere between 300 and 800 nm (Figure 2a). The pH 9.0 revealed a high level of synthesis, and the exceptional stability of the AgNPs led to their selection for future investigations. A similar observation was made by earlier studies, which reported that there was a slow rate of formation and aggregation of AgNPs at acidic pH [36,37]. On the other hand, it was observed that at basic pH, there was a possibility of Ag^+ precipitating as $AgNO_3$. Similar observations were made by other studies, which reported similar findings [33].

Table 1: Phytochemical analysis of *Cassia alata* flower extract

S. no.	Test	Results
1	Flavonoids	+
2	Phenols	+
3	Cardiac glycosides	+
4	Terpenoids	+
5	Glycosides	+
6	Anthraquinones	+
7	Quinones	+

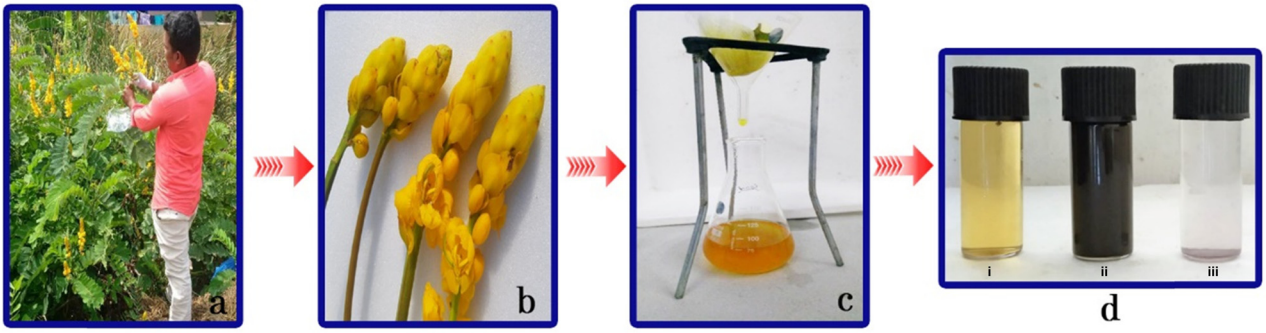

Figure 1: (a) Collection of *C. alata* flower; (b) flower petals; (c) aqueous flower petal extract; and (d) extract (i), reaction mixture (silver ion + extract) (ii), and silver ion alone (iii).

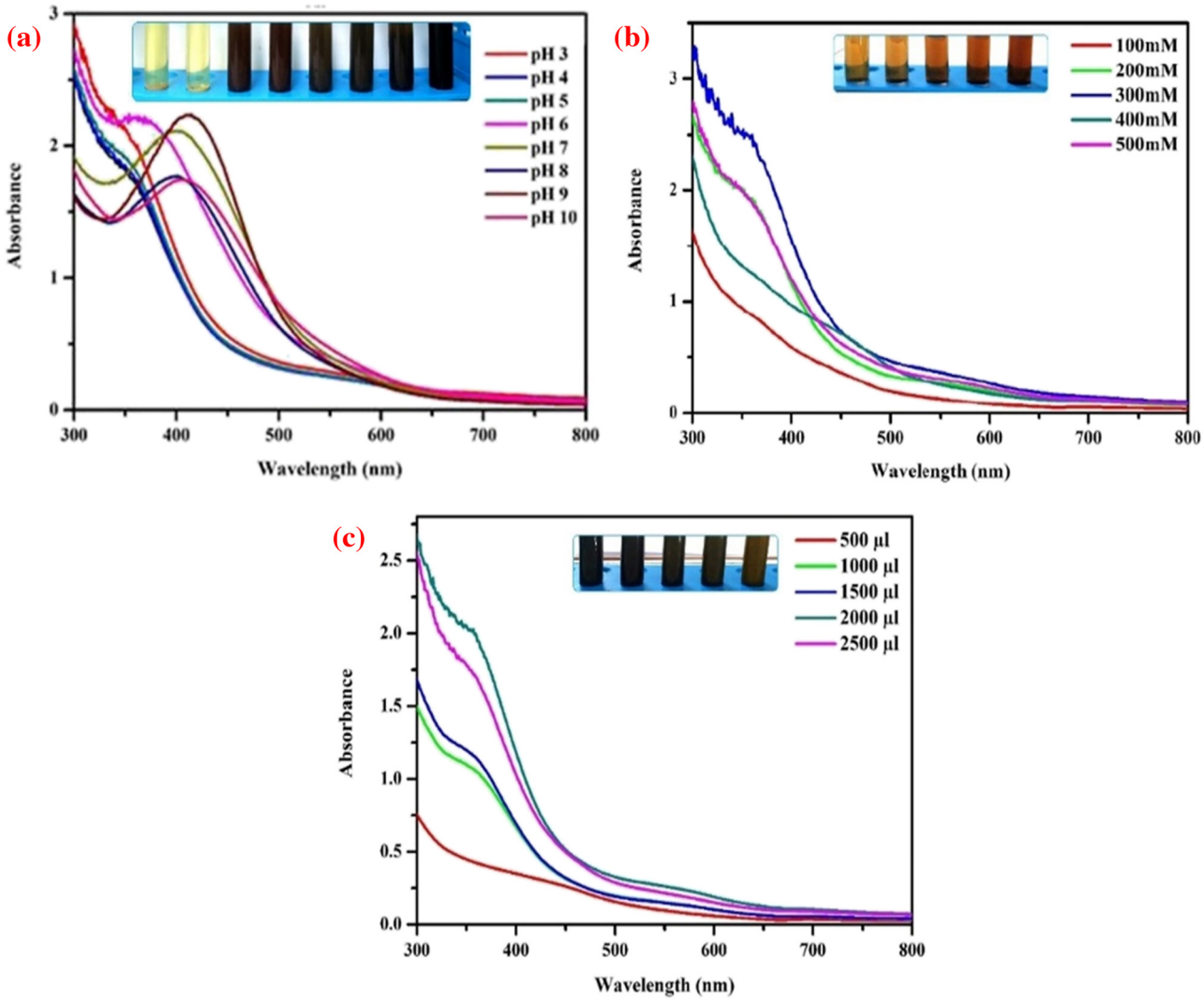

Figure 2: (a) Synthesis of AgNPs in different pH conditions and the inset image shows the reaction mixture. (b) Synthesis of AgNPs in different concentrations of silver ions and the inset image shows the reaction mixture. (c) Synthesis of AgNPs in different flower petal extract concentrations ions and the inset image shows the reaction mixture.

3.3 Examination of the impact of $AgNO_3$ concentrations

The brown color changes were observed (Figure 2b) in various concentrations of $AgNO_3$ from 100 to 500 mM. The absorbance of the resulting solutions was measured by the UV-Vis spectrophotometer (Figure 2b). Among them, 0.1 mM showed a high synthesis of AgNPs, and good stability was selected for further studies. These results agreed with the earlier investigations made by researchers [38,39], who reported that 1.0 mM silver ion concentration was the best for synthesizing AgNPs using *C. alata* plant flower extract.

3.4 Examination of flower extract concentrations

The brown color has been seen (Figure 2c) in varying concentrations of the substrate, ranging from 0.5 to 2.5 mL. Using a UV-Vis spectrophotometer, the absorbance of the resultant solutions was determined (Figure 2c). In particular, the addition of 0.1 mM solution to 2 mL of floral extract resulted in the maximum amount of biosynthesis of NPs. As a result, this particular combination was selected for further experiments. The elevations showed a consistent expansion all the way up to 450 nm, and this was provoked by slowly adding 1.5–2.5 mL of the solution. However, 1.0 mL of leaf extracts exhibited great stability in comparison to the other concentrations according to Timothy et al. [40] who revealed that several quantities of Tansy fruit were used to synthesize AgNPs and AuNPs. These concentrations included 0.5, 1.0, 1.8, 2.8, 3.8, and 4.8 mL, and it was determined that 1.0 mL was the optimal concentration for the creation of NPs.

3.5 Characterization of synthesized AgNPs

3.5.1 FTIR

FTIR analysis was carried out in order to determine which functional group of the biomolecule should be used to synthesize the AgNPs (Figure 3a). The findings of the FTIR analysis performed in this study reveal various lengths of bond stretches, which may be seen at various distant peaks. The H–OH stretching of phenols was corresponding to the band that could be seen at 3,465 cm^{-1} in the spectrum. The C═O stretching that occurs in aldehydes and ketones can be identified by the adsorption of the band at 1,635 cm^{-1}. The N═O bending of nitro groups is corresponding to the peak at 1,678 cm^{-1} in frequency. The C–O stretching of esters is reflected in the band that was found at a frequency of 1,008 cm^{-1}. The C–H stretching of alkenes is shown by the peaks that can be seen at 845 cm^{-1}.

3.5.2 TEM

The TEM was used to characterize the morphology and particle size of AgNPs. The TEM pictures of the AgNPs that were manufactured with the flower extract of *C. alata* indicated that they are primarily spherical and range in size from 20 to 100 nm (Figure 3c). According to the findings of Aissa et al., Murugan and Parimelazhagan [41,42], copper nanoparticles (CuNPs) with size ranging from 3.5 nm to 11 nm and the AgNPs had a spherical shape and measured between 17 and 29 nm. Additionally, researchers contrasted and examined the anticancer potential of gold nanoparticles (GNPs) on HeLa cell lines. The proteins, phenols, flavonoids, and aflatoxins found in Tulsi leaf preparations aid in reduction and stabilization, producing fluorescent GNPs that are quite stable, uniform, and tiny in size. Studies using MTT, reactive oxygen species (ROS), and mitochondrial membrane depolarization demonstrated that the synthesized GNPs efficiently and dose-dependently suppressed the proliferation and development of cell types [43].

3.5.3 EDX

The EDX spectrum reveals, as seen in Figure 3b, peaks that correspond to the individual elements that make up the actual composition of the sample. The existence of silver is confirmed by the fact that the elemental profile of the produced NPs has the largest X-ray energy peak at 3 keV, which is caused by silver. The elemental profile of the synthesized NPs is very similar to the elemental profile of silver, and the largest X-ray energy peak at 3 keV due to silver indicates the existence of silver.

3.5.4 XRD analysis

The crystalline nature of the green AgNPs that were generated by *C. alata* flower extract was also verified by XRD patterns analysis. The XRD pattern acquired for the AgNPs were produced by employing the aqueous floral extract of *C. alata*. The XRD examination was able to establish the AgNPs' crystalline nature as well as their size and phase identification. It demonstrated strong and distinct peaks at the following angles: 2θ = 38.05°, 45.6°, 47.27°, 66.2°, 68.9°, and 77.41° (Figure 3d). The XRD pattern revealed

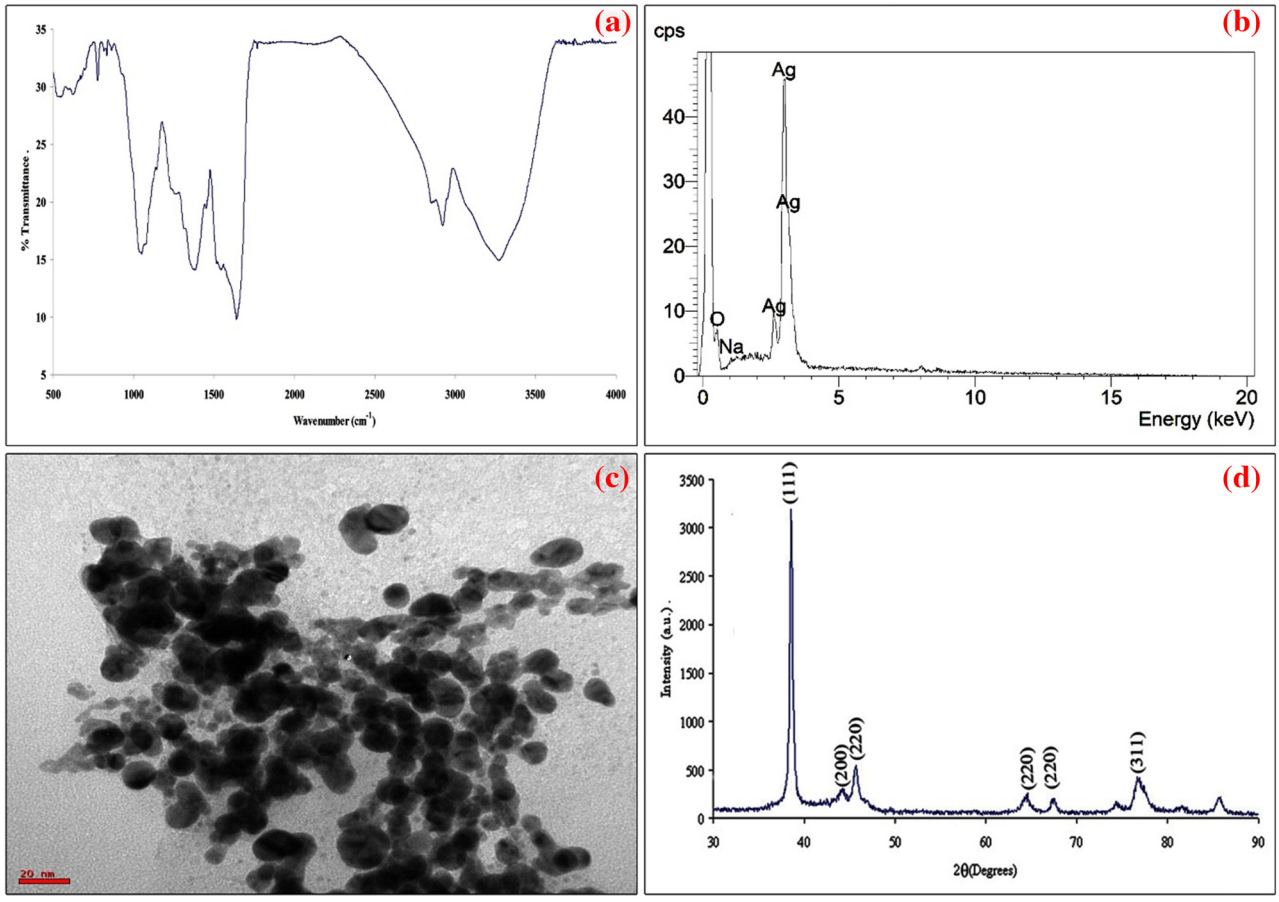

Figure 3: (a) FTIR spectra analysis of AgNPs. (b) HR-TEM image of AgNPs. (c) EDX of AgNPs. (d) XRD analysis.

that four diffraction peaks, 32.05, 46.27, 55.25, and 57.39°, could be indexed to the 111, 200, 220, and 311 planes of the face-centered cubic (FCC) crystalline silver, respectively [44]. By finding the complete width at half maximum of the Bragg's reflection corresponding to the (111) crystalline structure of AgNPs, the Debye–Schreyer equation was utilized to compute the average size of AgNPs. This was done by calculating the size of the AgNPs. The results obtained from the XRD experiment are in agreement with those that were previously published for the FCC lattice of silver [45].

3.6 Antifungal activity of flower extract and synthesized AgNPs

3.6.1 Well diffusion method

The antifungal effect of flower extract and AgNPs at different concentrations (50 and 100 µg) were quantitatively assessed based on the zone of inhibition (Tables 2 and 3). The maximum area of inhibition was observed in AgNPs, which exhibited an excellent effect on *T. rubrum* (28 ± 0.89 mm), followed by *E. floccosum*, (27 ± 0.62 mm), *A. fumigatus* (24 ± 0.43 mm), *C. albicans* (22 ± 0.67 mm), and *Mucor* sp. (22 ± 0.48 mm) (Figure 4) and the zone of inhibition of flower extract against *E. floccosum* (21 ± 1.23 mm) followed by *Mucor* sp. (21 ± 1.87 mm), *E. floccosum* (21 ± 1.54 mm), *C. albicans* (19 ± 1.42 mm), and *A. fumigatus* (18 ± 1.45 mm) (Figure 4). A comparison was made between the zone of inhibition and the conventional antifungal drug nystatin.

Table 2: Antifungal activity of *C. alata* flower extract

S. no.	Fungal pathogens	Zone of inhibition (mm)		
		Concentration of flower extract		Positive control (nystatin)
		50 µL	100 µL	
1	*A. fumigates*	14 ± 1.56	18 ± 1.45	14 ± 0.23
2	*C. albicans*	14 ± 1.32	19 ± 1.42	22 ± 0.25
3	*Mucor* sp.	15 ± 2.12	21 ± 1.87	22 ± 0.23
4	*T. rubrum*	15 ± 2.32	21 ± 1.23	19 ± 0.24
5	*E. floccosum*	16 ± 1.98	21 ± 1.54	13 ± 0.25

Table 3: Antifungal activity of AgNPs

S. no.	Fungal pathogens	Zone of inhibition (mm)		
		Concentration of AgNPs		Positive control (nystatin)
		50 µL	100 µL	
1	*A. fumigates*	19 ± 0.98	24 ± 0.43	14 ± 0.23
2	*C. albicans*	18 ± 0.24	22 ± 0.67	22 ± 0.25
3	*Mucor* sp.	20 ± 0.35	22 ± 0.48	22 ± 0.23
4	*T. rubrum*	23 ± 1.23	28 ± 0.89	19 ± 0.24
5	*E. floccosum*	22 ± 0.43	27 ± 0.62	13 ± 0.25

3.6.2 MFC

The MFC of flower extract was revealed by the mean diameter of the zone of inhibitions against dermatophytes. MFC values were recorded at 20.0, 25.0, and 30.0 µL·mL^{-1} against *T. rubrum* (20 ± 0.67 mm), *E. floccosum* (27 ± 0.62 mm), *A. fumigatus* (24 ± 0.43 mm), *C. albicans* (22 ± 0.67 mm), and *Mucor* sp. (22 ± 0.48 mm), respectively.

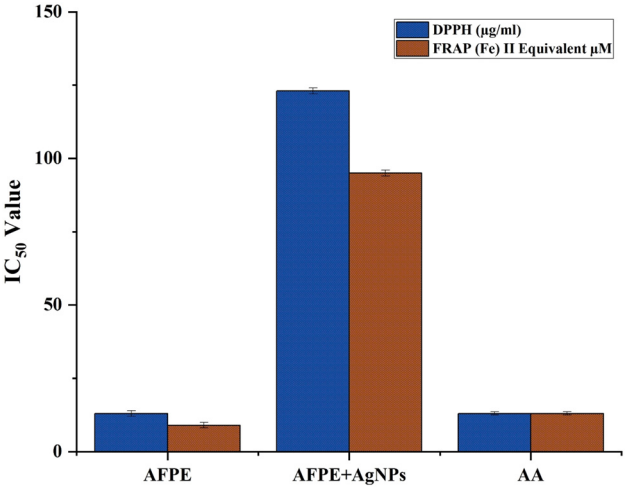

Figure 5: DPPH and FRAP free radical scavenging activity of synthesized AgNPs.

3.7 Antioxidant activity of flower extract and synthesized AgNPs

Antioxidants are chemicals that scavenge free radicals and shield people from degenerative illnesses including

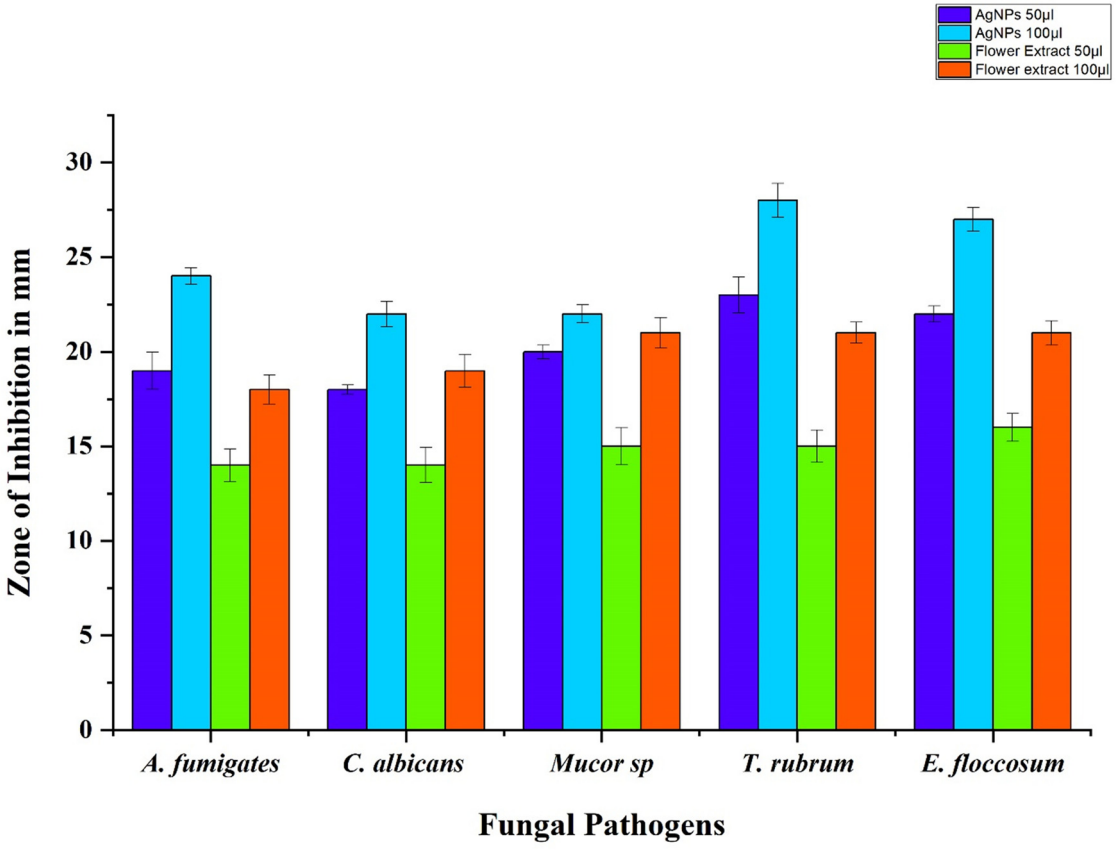

Figure 4: Antifungal activity of AgNPs and *C. alata* flower extract.

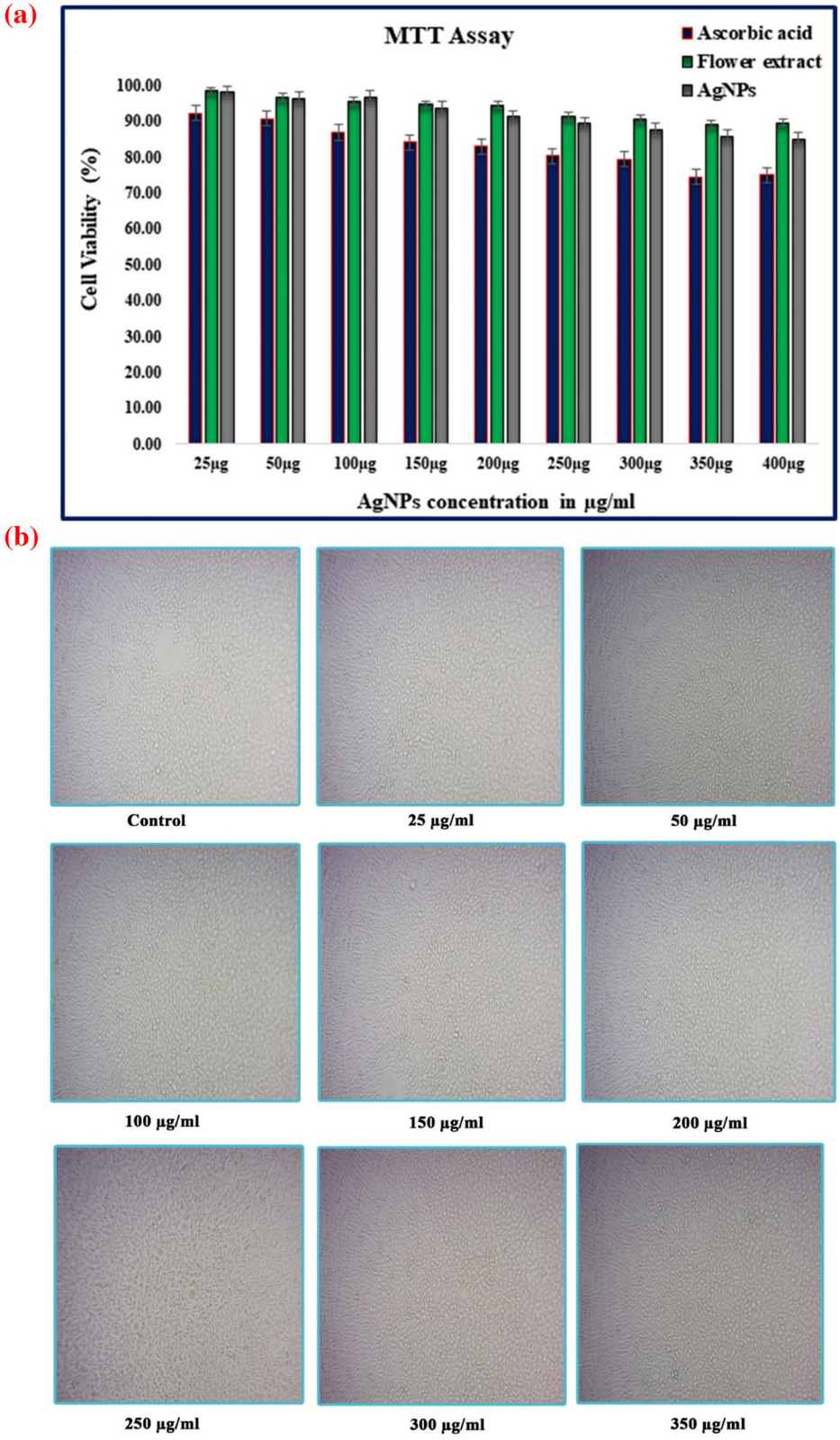

Figure 6: (a and b) MTT assay using human fibroblast cell line L929.

cancer, Parkinson's, Alzheimer's, and atherosclerosis that are brought on by oxidative stress (overproduction of the free radicals) [35]. The phenolic chemicals found in medicinal plants, such as phenolic acids and flavonoids, donate their hydrogen atom and are in charge of scavenging free radicals (ROS) [46]. Through DPPH and FRAP experiments, the results of the current study demonstrated the antioxidant capacity of AgNPs at varied doses (10–100 $g \cdot mL^{-1}$) (Figure 5). The outcome showed that the percentage inhibition rose when the concentration of AgNPs, flower aqueous extract, and ascorbic acid increased from 20 to 100 $g \cdot mL^{-1}$ (Figure 5). In the DPPH assay, the higher antioxidant activity was observed at higher concentrations of AgNPs and ascorbic acid as 44.80 and 70.80 $\mu g \cdot mL^{-1}$, respectively, whereas for FRAP assays, the values were 46.30 $\mu M \cdot mL^{-1}$ $FeSO_4$ equivalents, 110.22 $\mu M \cdot mL^{-1}$ $FeSO_4$ equivalents, and 6.34 $\mu M \cdot mL^{-1}$ $FeSO_4$ equivalents, respectively. Ascorbic acid displayed the lowest antioxidant activity in the DPPH and FRAP experiments, followed by AgNPs. The increased antioxidant capacity may be a result of the higher polyphenolic content of the flower extract that capped on AgNPs [47]. AgNPs demonstrated a wide range of antioxidant activity in all of these investigations by successfully suppressing the reactive oxygen species [48].

3.8 Cell line

The synthesized AgNPs' cytotoxicity was examined by *in vitro* method using L929 cell line. Different concentrations of AgNPs (25–1,200 $\mu g \cdot mL^{-1}$) were treated with cell line for 24 h and compared with the control DMEM. MTT and other chemicals changed into yellow color depending on the metabolic activities inside the cell because of the enzyme cellular oxidoreductase [49]. Although the results of this systematic review demonstrated that biogenic AuNPs have a significant anticancer potential against cervical cancer cells, many difficulties and ambiguities need to be clarified in subsequent research, including the location of these NPs in the body, their acute and chronic toxicity towards other normal tissues, their genotoxicity, immunogenicity, and other issues [50]. The viability of the cells and the IC_{50} value of 50 $\mu g \cdot mL^{-1}$ were reduced sharply. Based on the cell line result, the low concentration of AgNPs showed a 98% cell viability compared to other concentrations. Morphology changes were observed in high density due to the enhanced cytotoxic effect (Figure 6a and b).

4 Conclusion

Biomedical repair of skin illness utilizing nano-produced AgNPs offers frequent and economic yield-increasing technological applications. Antimicrobial materials contain natural and inorganic components. Metal NPs have been extensively investigated due to their unique physicochemical properties and large specific surface area. AgNPs from plant extracts have antimicrobial properties. In our study, *C. alata* aqueous flower extract was utilized to produce AgNPs, demonstrating the flower's efficiency as a natural, low-cost silver bio-reduction agent. UV-Vis, FTIR, SEM, EDX, and XRD characterizations were carried out. Using aqueous *C. alata*, we produced 20 nm spherical AgNPs. Flower extract produced small, crystalline AgNPs. They established their biomedical value by fighting skin infections. The study shows 98% cell line viability. AgNPs are used in the biomedical and pharmaceutical industries to make antifungal skin ointments and cytotoxic drugs.

Funding information: This work was supported by the National Research Foundation of Korea (NRF) grant funded by the Korean Government (MSIT) (No. 2021054783). The authors extend their appreciation to the Researchers Supporting Project Number (RSP2023R143), King Saud University, Riyadh, Saudi Arabia.

Author contributions: Moorthy Muruganandham: conceptualization, investigation, data collection, formal analysis, methodology, writing – original draft, and visualization; Kanagasabapathy Sivasubramanian: conceptualization, formal analysis, supervision, and visualization; Abdulrahman I. Almansour: formal analysis and methodology; Natarajan Arumugam: formal analysis and methodology; Palanivel Velmurugan and Subpiramaniyam Sivakumar: formal analysis and writing – review and editing; Raju Suresh Kumar and Sakkarapalayam M. Mahalingam: project administration, conceptualization, supervision, formal analysis, methodology, validation, writing – original draft, writing – review and editing, and visualization.

Conflict of interest: Authors state no conflict of interest.

References

[1] Basak S, Singh P, Rajurkar M. Multidrug resistant and extensively drug resistant bacteria: A study. J Pathog. 2016;2016:1–5. doi: 10.1155/2016/4065603.

[2] Ahn EY, Jin H, Park Y. Assessing the antioxidant, cytotoxic, apoptotic and wound healing properties of silver nanoparticles green-synthesized by plant extracts. Mater Sci Eng C. 2019;101:204–16. doi: 10.1016/j.msec.2019.03.095.
[3] Fahimirad S, Ajalloueian F, Ghorbanpour M. Synthesis and therapeutic potential of silver nanomaterials derived from plant extracts. Ecotoxicol Environ Saf. 2019;168:260–78. doi: 10.1016/j.ecoenv.2018.10.017.
[4] Haggag EG, Elshamy AM, Rabeh MA, Gabr NM, Salem M, Youssif KA, et al. Antiviral potential of green synthesized silver nanoparticles of *Lampranthus coccineus* and *Malephora lutea*. Int J Nanomed. 2019;14:6217–29. doi: 10.2147/IJN.S214171.
[5] Totaro P, Rambaldini M. Efficacy of antimicrobial activity of slow release silver nanoparticles dressing in post-cardiac surgery mediastinitis. Interact Cardiovasc Thorac Surg. 2009;8(1):153–4. doi: 10.1510/icvts.2008.188870.
[6] Kruis FE, Fissan H, Rellinghaus B. Sintering and evaporation characteristics of gas-phase synthesis of size-selected PbS nanoparticles. Mater Sci Eng B. 2000;69:329–34. doi: 10.1016/S0921-5107(99)00298-6.
[7] Magnusson MH, Deppert K, Malm JO, Bovin JO, Samuelson L. Gold nanoparticles: production, reshaping, and thermal charging. J Nanopart Res. 1999;1:243–51. doi: 10.1023/A:1010012802415.
[8] Wiley B, Herricks T, Sun Y, Xia Y. Polyol synthesis of silver nanoparticles: use of chloride and oxygen to promote the formation of single-crystal, truncated cubes and tetrahedrons. Nano Lett. 2004;4(9):1733–9. doi: 10.1021/nl048912c.
[9] Guzmán MG, Dille J, Godet S. Synthesis of silver nanoparticles by chemical reduction method and their antibacterial activity. Int J Chem Biomol Eng. 2009;2(3):104–11.
[10] Song KC, Lee SM, Park TS, Lee BS. Preparation of colloidal silver nanoparticles by chemical reduction method. Korean J Chem Eng. 2009;26:153–5. doi: 10.1007/s11814-009-0024-y.
[11] Rashid MU, Bhuiyan MK, Quayum ME. Synthesis of silver nano particles (Ag-NPs) and their uses for quantitative analysis of vitamin C tablets. Dhaka Univ J Pharm Sci. 2013;12(1):29–33. doi: 10.3329/dujps.v12i1.16297.
[12] Ahmed S, Ahmad M, Swami BL, Ikram S. A review on plants extract mediated synthesis of silver nanoparticles for antimicrobial applications: a green expertise. J Adv Res. 2016;7(1):17–28. doi: 10.1016/j.jare.2015.02.007.
[13] Prasad R. Synthesis of silver nanoparticles in photosynthetic plants. J Nanopart. 2014;2014:1–8. doi: 10.1155/2014/963961.
[14] Barabadi H, Mojab F, Vahidi H, Marashi B, Talank N, Hosseini O, et al. Green synthesis, characterization, antibacterial and biofilm inhibitory activity of silver nanoparticles compared to commercial silver nanoparticles. Inorg Chem Commun. 2021;129:108647. doi: 10.1016/j.inoche.2021.108647.
[15] Barabadi H, Mostafavi E, Truong LB, Cruz DM, Vahidi H, Mahjoub MA, et al. Microbial nanotechnology–based approaches for wound healing and infection control. Handbook of Microbial Nanotechnology. UK: Academic Press; 2022. p. 1–15. doi: 10.1016/B978-0-12-823426-6.00009-7.
[16] Talank N, Morad H, Barabadi H, Mojab F, Amidi S, Kobarfard F, et al. Bioengineering of green-synthesized silver nanoparticles: In vitro physicochemical, antibacterial, biofilm inhibitory, anticoagulant, and antioxidant performance. Talanta. 2022;243:123374. doi: 10.1016/j.talanta.2022.123374.
[17] Barabadi H, Jounaki K, Pishgahzadeh E, Morad H, Sadeghian-Abadi S, Vahidi H, et al. Antiviral potential of green-synthesized silver nanoparticles. Handbook of Microbial Nanotechnology. UK: Academic Press; 2022. p. 285–310. doi: 10.1016/B978-0-12-823426-6.00030-9.
[18] Barabadi H, Hosseini O, Damavandi Kamali K, Jazayeri Shoushtari F, Rashedi M, Haghi-Aminjan H, et al. Emerging theranostic silver nanomaterials to combat lung cancer: A systematic review. J Clust Sci. 2020;31:1–10. doi: 10.1007/s10876-019-01639-z.
[19] Barabadi H, Vahidi H, Damavandi Kamali K, Rashedi M, Hosseini O, Golnaraghi Ghomi AR, et al. Emerging theranostic silver nanomaterials to combat colorectal cancer: A systematic review. J Clust Sci. 2020;31:311–21. doi: 10.1007/s10876-019-01668-8.
[20] Mostafavi E, Zarepour A, Barabadi H, Zarrabi A, Truong LB, Medina-Cruz D. Antineoplastic activity of biogenic silver and gold nanoparticles to combat leukemia: beginning a new era in cancer theragnostic. Biotechnol Rep. 2022;34:e00714. doi: 10.1016/j.btre.2022.e00714.
[21] Barabadi H, Vahidi H, Rashedi M, Mahjoub MA, Nanda A, Saravanan M. Recent advances in biological mediated cancer research using silver nanoparticles as a promising strategy for hepatic cancer therapeutics: A systematic review. Nanomed J. 2020;7(4):251–62. doi: 10.22038/NMJ.2020.07.00001.
[22] Sule WF, Okonko IO, Omo-Ogun S, Nwanze JC, Ojezele MO, Ojezele OJ, et al. Phytochemical properties and in-vitro antifungal activity of *Senna alata* Linn. crude stem bark extract. J Med Plants Res. 2011;5(2):176–83. doi: 10.5897/JMPR.9001002.
[23] Amao EA, Adeoti TM, Ayandele B, Jimoh AR. Clinical response of broilers placed on varying levels of aqueous *Cassia alata* leaf extract. J Med Plants Res. 2014;8(12):520–2. doi: 10.5897/JMPR2013.4464.
[24] Ameen M. Epidemiology of superficial fungal infections. Clin Dermatol. 2010;28(2):197–201. doi: 10.1016/j.clindermatol.2009.12.005.
[25] Jayasree R, Prathiba R, Sangavi S. Immunomodulatory effect of Cassia alata petals in Garra rufa (doctor fish). J Chem Pharm Sci. 2016;9(1):215–8.
[26] Netala VR, Kotakadi VS, Domdi L, Gaddam SA, Bobbu P, Venkata SK, et al. Biogenic silver nanoparticles: Efficient and effective antifungal agents. Appl Nanosci. 2016;6:475–84. doi: 10.1007/s13204-015-0463-1.
[27] Manikandan V, Velmurugan P, Park JH, Chang WS, Park YJ, Jayanthi P, et al. Green synthesis of silver oxide nanoparticles and its antibacterial activity against dental pathogens. 3 Biotech. 2017;7:1–9. doi: 10.1007/s13205-017-0670-4.
[28] Indumathi T, Theivarasu C, Pradeep I, Rani MT, Magesh G, Rahale CS, et al. Effects of Nd doping on structural, optical, morphological and surface-chemical state analysis of ZnO nanoparticles for antimicrobial and anticancer activities. Surf Interfaces. 2021;23:101000. doi: 10.1016/j.surfin.2021.101000.
[29] Boulc'h F, Schouler MC, Donnadieu P, Chaix JM, Djurado E. Domain size distribution of Y-TZP nano-particles using XRD and HRTEM. Image Anal Stereol. 2001;20(3):157–61. doi: 10.5566/ias.v20.p157-161.
[30] Guerra F, Ansari AA, Kurup R, Subramanian G. Antifungal activity of *Senna alata*, *Senna bicapsularis* and *Pityrogramma*

calomelanos. J Complement Altern Med Res. 2020;10(3):11–21. doi: 10.9734/jocamr/2020/v10i330164.
[31] Varghese GK, Bose LV, Habtemariam S. Antidiabetic components of *Cassia alata* leaves: identification through α-glucosidase inhibition studies. Pharm Biol. 2013;51(3):345–9. doi: 10.3109/13880209.2012.729066.
[32] Singhal G, Bhavesh R, Kasariya K, Sharma AR, Singh RP. Biosynthesis of silver nanoparticles using *Ocimum sanctum* (Tulsi) leaf extract and screening its antimicrobial activity. J Nanopart Res. 2011;13:2981–8. doi: 10.1007/s11051-010-0193-y.
[33] Doughari JH, Okafor B. Antimicrobial activity of *Senna alata* Linn. East Cent Afr J Pharm Sci. 2007;10(1):17–21. doi: 10.4314/ecajps.v10i1.9756.
[34] Balashanmugam P, Kalaichelvan PT. Biosynthesis characterization of silver nanoparticles using *Cassia roxburghii* DC. aqueous extract, and coated on cotton cloth for effective antibacterial activity. Int J Nanomed. 2015;10(sup2):87–97. doi: 10.2147/IJN.S79984.
[35] Lal S, Verma R, Chauhan A, Dhatwalia J, Guleria I, Ghotekar S, et al. Antioxidant, antimicrobial, and photocatalytic activity of green synthesized ZnO-NPs from *Myrica esculenta* fruits extract. Inorg Chem Commun. 2022;141:109518.
[36] Morones JR, Elechiguerra JL, Camacho A, Holt K, Kouri JB, Ramírez JT, et al. The bactericidal effect of silver nanoparticles. Nanotechnology. 2005;16(10):2346. doi: 10.1088/0957-4484/16/10/059.
[37] Sun C, Lee JS, Zhang M. Magnetic nanoparticles in MR imaging and drug delivery. Adv Drug Deliv Rev. 2008;60(11):1252–65. doi: 10.1016/j.addr.2008.03.018.
[38] Mock JJ, Barbic M, Smith DR, Schultz DA, Schultz S. Shape effects in plasmon resonance of individual colloidal silver nanoparticles. J Chem Phys. 2002;116(15):6755–9. doi: 10.1063/1.1462610.
[39] Krishnaraj C, Ramachandran R, Mohan K, Kalaichelvan PT. Optimization for rapid synthesis of silver nanoparticles and its effect on phytopathogenic fungi. Spectrochim Acta A Mol Biomol Spectrosc. 2012;93:95–9. doi: 10.1016/j.saa.2012.03.002.
[40] Timothy SY, Wazis CH, Adati RG, Maspalma ID. Antifungal activity of aqueous and ethanolic leaf extracts of *Cassia alata* Linn. J Appl Pharm Sci. 2012;2(7):182–5. doi: 10.7324/JAPS.2012.2728.
[41] Aissa MA, Tremblay B, Andrieux-Ledier A, Maisonhaute E, Raouafi N, Courty A. Copper nanoparticles of well-controlled size and shape: A new advance in synthesis and self-organization. Nanoscale. 2015;7(7):3189–95. doi: 10.1039/C4NR06893A.
[42] Murugan R, Parimelazhagan T. Comparative evaluation of different extraction methods for antioxidant and anti-inflammatory properties from *Osbeckia parvifolia* Arn.–An *in vitro* approach. J King Saud Univ Sci. 2014;26(4):267–75. doi: 10.1016/j.jksus.2013.09.006.
[43] Virmani I, Sasi C, Priyadarshini E, Kumar R, Sharma SK, Singh GP, et al. Comparative anticancer potential of biologically and chemically synthesized gold nanoparticles. J Clust Sci. 2020;31:867–76. doi: 10.1007/s10876-019-01695-5.
[44] Bankalgi SC, Londonkar RL, Madire U, Tukappa NA. Biosynthesis, characterization and antibacterial effect of phenolics-coated silver nanoparticles using *Cassia javanica* L. J Clust Sci. 2016;27:1485–97. doi: 10.1007/s10876-016-1016-9.
[45] Dubey SP, Lahtinen M, Sillanpää M. Tansy fruit mediated greener synthesis of silver and gold nanoparticles. Process Biochem. 2010;45(7):1065–71. doi: 10.1016/j.procbio.2010.03.024.
[46] Tarhan L, Urek RO, Oner A, Nakiboglu M. Evaluation of phenolic profiles, antioxidant activities, and cytotoxic and apoptotic potentials of *Phlomis angustissima* and *Phlomis fruticosa*, medicinal plants from Turkey. Eur J Integr Med. 2022;55:102188. doi: 10.1016/j.eujim.2022.102188.
[47] Labulo AH, David OA, Terna AD. Green synthesis and characterization of silver nanoparticles using *Morinda lucida* leaf extract and evaluation of its antioxidant and antimicrobial activity. Chem Pap. 2022;16:1–3. doi: 10.1007/s11696-022-02392-w.
[48] Moorthy K, Chang KC, Yu PJ, Wu WJ, Liao MY, Huang HC, et al. Synergistic actions of phytonutrient capped nanosilver as a novel broad-spectrum antimicrobial agent: unveiling the antibacterial effectiveness and bactericidal mechanism. N J Chem. 2022;46(32):15301–12. doi: 10.1039/D2NJ02469A.
[49] Berridge MV, Herst PM, Tan AS. Tetrazolium dyes as tools in cell biology: new insights into their cellular reduction. Biotechnol Annu Rev. 2005;11:127–52. doi: 10.1016/S1387-2656(05)11004-7.
[50] Barabadi H, Vahidi H, Mahjoub MA, Kosar Z, Damavandi Kamali K, Ponmurugan K, et al. Emerging antineoplastic gold nanomaterials for cervical cancer therapeutics: A systematic review. J Clust Sci. 2020;31:1173–84. doi: 10.1007/s10876-019-01733-2.